Studies of Perturbation Theory and Spin Temperature by Rotary Saturation of Spins*

JUDY R. FRANZ† AND CHARLES P. SLICHTER
Department of Physics and Materials Research Laboratory, University of Illinois, Urbana, Illinois
(Received 9 March 1966)

The relationship between the Bloembergen-Purcell-Pound theory of resonance saturation and the Redfield theory is discussed in terms of the effect of a weak perturbation acting for a long time on a spin system perfectly isolated from the lattice. A simple derivation of Provotorov's rate equations is given, based on Schumacher's concepts. The theoretical ideas are applied to the F^{19} resonance in CaF_2 to discuss the phenomenon of rotary saturation, in which one applies a radio-frequency field H_1, and modulates the static field at a frequency ω_a such that $\gamma H_1 \cong \omega_a$, where γ is the nuclear gyromagnetic ratio. When H_1 is large compared to the local field, the rotary saturation is described by Redfield's concepts; when H_1 is comparable to the local field, the original Bloembergen-Purcell-Pound theory works.

I. INTRODUCTION

In a magnetic-resonance experiment, the absorption of energy from the applied radio-frequency field produces either an increase in the energy of the spin system or a transfer of energy from the spin system to the lattice. Since the latter process requires a time interval of the order of the spin-lattice relaxation time T_1 one can be assured that on a short enough time scale following the turn-on of the radio-frequency field, the absorption of energy will go into raising the energy of the spin system. In general, as the spin energy rises, the absorption rate decreases until an equilibrium is reached. The situation we have described (saturation) was analyzed by Bloembergen, Purcell, and Pound,[1] as well as by Bloch,[2] but in 1955 Redfield[3] discovered that the equilibrium state they predicted was not in fact correct. He gave a successful theory. In his analysis he considered experiments on a time scale long compared with T_1, for which the heat flow to the lattice must be taken into account. Subsequently, Goldburg[4] and Slichter and Holton[5] used Redfield's theory to analyze the equilibrium obtained for times less than T_1 (which enabled them to neglect the role of the lattice), and verified the predictions experimentally. A theoretical analysis of the approach to equilibrium was given by Provotorov,[6] neglecting the lattice, and was subsequently verified in part by Goldburg[4] and Walstedt.[7]

One of the conditions of validity of Redfield's theory was that the applied static field H_0 be much stronger than either the applied radio-frequency field H_1 or the local field H_L, the field at one nucleus produced by its neighbors. In this paper we give a simple derivation of the Provotorov equations and study experimentally the approach to equilibrium in both the limits of strong and weak static fields. We find that in the weak-field limit, the Redfield theory breaks down, as is to be expected, but that a BPP theory successfully accounts for the experiments.

The absorption spectrum in a weak static field has been studied previously by Anderson.[8] He used the saturation method and made the assumption that at all times the spin system was described by a spin temperature. For static fields somewhat larger than the linewidth, he found deviations which he ascribed to the onset of the Redfield condition, i.e., the spins were more appropriately assigned a temperature in the rotating reference frame.

Our experiments were actually instituted to understand the phenomena Redfield called rotary saturation. We apply a strong static field H_0, an alternating field H_1, and "view" the problem in a reference frame rotating with H_1. In this reference frame, H_1 becomes the static field, which can be made large or small compared to the local field. To produce "rotary saturation," H_0 is modulated at an audio frequency ω_a to induce transitions in the spin system. This technique is of great practical utility for calibrating the strength of H_1, since when $\gamma H_1 = \omega_a$ one expects the audio-frequency field to induce spin transitions (where γ is the nuclear gyromagnetic ratio). Thus the simple measurement of frequency (ω_a) gives one a precise calibration of H_1. What we find is that we can achieve a very detailed quantitative understanding by applying the spin temperature concepts to an appropriately chosen rotating reference frame.

II. THEORY

We consider a system of nuclear spins that interact only with each other through their magnetic-dipolar coupling and with applied magnetic fields. Then the Hamiltonian of the system can be written

$$\mathcal{H} = \mathcal{H}_z + \mathcal{H}_d + \mathcal{H}_{rf}. \quad (1)$$

* This research was partially supported by the U. S. Atomic Energy Commission under Contract AT(11-1)-1198.
† Now at IBM Research Laboratory, Zurich, Switzerland.
[1] N. Bloembergen, E. M. Purcell, and R. V. Pound, Phys. Rev. **73**, 679 (1948). Throughout the rest of this paper we will refer to this article as BPP.
[2] C. P. Slichter, *Principles of Magnetic Resonance* (Harper and Row Publishers, New York, 1963), Chap. 2.
[3] A. G. Redfield, Phys. Rev. **98**, 1787 (1955).
[4] W. I. Goldburg, Phys. Rev. **128**, 1554 (1962).
[5] C. P. Slichter and W. C. Holton, Phys. Rev. **122**, 1701 (1961).
[6] B. N. Provotorov, Zh. Eksperim. i Teor. Fiz. **41**, 1582 (1961) [English transl.: Soviet Phys.—JETP **14**, 1126 (1962)].
[7] R. E. Walstedt, Phys. Rev. **138**, A1096 (1965).
[8] A. G. Anderson, Phys. Rev. **125**, 1517 (1962).

$\mathcal{H}_z$ is the Zeeman interaction,

$$\begin{aligned}\mathcal{H}_z &= -\gamma\hbar H_0 \sum_j I_{zj} \\ &= -\gamma\hbar H_0 I_z ,\end{aligned} \tag{2}$$

where H_0 is the static field applied in the z direction and I_z is the total z component of the spin. $\mathcal{H}_d$ is the spin-spin interaction,

$$\mathcal{H}_d = \hbar^2\gamma^2 \sum_{k>j} \left[\frac{\mathbf{I}_j \cdot \mathbf{I}_k}{r_{jk}^3} - 3\frac{(\mathbf{I}_j \cdot \mathbf{r}_{jk})(\mathbf{I}_k \cdot \mathbf{r}_{jk})}{r_{jk}^5} \right], \tag{3}$$

where r_{jk} is the vector distance from spin j to spin k. $\mathcal{H}_{rf}$ gives the interaction of the spins with an applied radio-frequency magnetic field that is perpendicular to H_0, of frequency ω and amplitude $2H_1$.

$$\mathcal{H}_{rf} = -\gamma\hbar 2H_1 \sum I_{jx} \cos\omega t. \tag{4}$$

The complete solution of Eq. (1) is very difficult, but various approximate treatments have been given. Bloembergen, Purcell, and Pound[1] treated the problem using perturbation theory in 1948. They showed that the population difference n between the two energy levels of a system of spin-$\frac{1}{2}$ particles is given by the differential equation,

$$dn/dt = -2W(\omega)n + (n_0 - n)/T_1, \tag{5}$$

where $W(\omega)$ is the probability/second that a spin will be flipped by the applied radio-frequency field, n_0 is the thermal equilibrium value of n, and T_1 is the spin-lattice relaxation time. For a spin-$\frac{1}{2}$ nucleus, standard perturbation theory gives

$$W(\omega) = (\pi/2)\gamma^2 H_1^2 f(\omega), \tag{6}$$

where $f(\omega)$ is the normalized line-shape function.

In this paper, we will consider only systems that interact very weakly with the lattice, so that the spin-lattice relaxation time is very long. In this case the second term on the right-hand side of Eq. (5) can be neglected, resulting in the very simple solution,

$$n = Ae^{-2W(\omega)t}, \tag{7}$$

where A is a constant of integration. However this solution involves $W(\omega)$ which is obtained from perturbation theory, so that its applicability is restricted by the conditions under which perturbation theory is valid.[2] There are two such conditions. The first is that the perturbation matrix elements be small compared to the width of the energy levels, a condition that can always be satisfied by making H_1 small enough. The second is that the wave function, and thus the populations of the energy levels, may not change appreciably during the application of the perturbation. The second is clearly violated in Eq. (7) for times longer than about $1/W$. In the limit of infinite spin-lattice relaxation times, no matter how weak the perturbing field is made, if it persists for a long enough time, the second condition will be violated. A new approach is therefore necessary to describe the behavior of a spin system when it is subjected to a perturbation of long duration.

In 1955 Redfield[3] found the solution to this problem. He was led by anomalous results in his measurements of the spin-lattice relaxation time in metals to make the following hypothesis: A spin system will achieve an equilibrium in the reference frame in which the time-dependent couplings of the system are effectively eliminated. He went on to show that for a spin system subjected to an rf field strong enough to produce saturation, the appropriate reference frame is one that rotates about the static field at the frequency of the rf field and in the sense of precession of the spins. In this rotating reference frame, the Hamiltonian in Eq. (1) becomes[3]

$$\mathcal{H}' = -\gamma\hbar\mathbf{H}_{\text{eff}} \cdot \sum_j \mathbf{I}_j + \gamma^2\hbar^2 \sum_{k>j} A_{jk}[\mathbf{I}_j \cdot \mathbf{I}_k - 3I_{jz}I_{kz}] + \text{terms oscillating at } \pm\omega, \pm 2\omega. \tag{8}$$

The first term gives the interaction of the spins with the effective static field in the rotating frame,

$$\begin{aligned}\mathbf{H}_{\text{eff}} &= H_1\mathbf{i} + [H_0 - \omega/\gamma]\mathbf{k} \\ &= H_1\mathbf{i} + h\mathbf{k}.\end{aligned} \tag{9}$$

The second term in Eq. (8) gives the static spin-spin interaction $\mathcal{H}_d^0$, that is, the part that commutes with I_z, and is therefore invariant under rotation about the z axis. A_{jk} is a constant that depends only on the lattice structure of the crystal. Although oscillating terms remain in the transformed Hamiltonian, these terms usually have no effect in the rotating frame. This can be seen as follows: In the rotating frame, the nuclei experience two types of fields, the effective static field H_{eff} which is a combination of the applied fields, and the local field H_L which can be defined quantitatively[5] in terms of $\text{Tr}(\mathcal{H}_d^0)^2$, the trace of the square of the spin-spin Hamiltonian in the rotating frame. The energy level splitting in the rotating frame will, therefore, be of the order of $\hbar\gamma[H_{\text{eff}}^2 + H_L^2]^{1/2}$. Since both H_{eff} and H_L are of the order of a few gauss, the splitting will be a few kc/sec. The oscillating terms have a frequency near the laboratory resonant frequency of order γH_0. For typical resonance experiments this is about 10 Mc/sec. Therefore the oscillating terms in the Hamiltonian are so far off resonance that they have no effect on the system. Only if $H_0 \approx H_{\text{eff}}$ or H_L will these terms become important. Thus, in the usual resonance experiment, the Hamiltonian in the rotating frame is time-independent, and Redfield's theory of an equilibrium in the rotating frame is valid. (The demonstration that there is a breakdown in the Redfield condition in low fields is, as we have remarked, one of the objectives of our experiments.)

More specifically, the equilibrium Redfield postulated was the usual one of thermodynamics, namely, that in the rotating reference frame one could assign a temperature θ to the spins, and that the population of the

energy levels of $\mathcal{H}'$ would be given by the Boltzmann factor at that temperature.

Using these ideas, Slichter and Holton[5] and Goldburg[4] found the equilibrium state which would be reached after the sudden turn-on of H_1. For the limit of small H_1, they found the equilibrium z component of magnetization was given by

$$(M_z)_{\text{eq}}=M_0\frac{h^2+H_L^2h/H_0}{H_{\text{eff}}^2+H_L^2}. \tag{10}$$

Since M_z is proportional to the population difference n, Eq. (10) shows that the BPP theory is incorrect in its prediction that n goes to zero for long times.

We are thus faced with the situation that we have a correct theory for short times (BPP), and we know the asymptotic value of M_z (from Redfield theory), but do not know how to find the behavior of M_z in between. Provotorov,[6] using powerful general methods, found the solution to this problem. It is possible, however, to derive his result in an equivalent manner which we believe helps shed light on the connection between BPP and Redfield theory.

To do so we note that for short times and small H_1, perturbation theory is valid. Using the proportionality between n and M_z, we therefore get from Eq. (5) (still assuming $T_1=\infty$)

$$dM_z/dt=-2W(\omega)M_z. \tag{11}$$

In the absence of H_1, the Zeeman interaction in the rotating frame is just

$$\mathcal{H}_z=-\gamma hhI_z. \tag{12}$$

Philippot[9] has shown that in the high-temperature limit the Zeeman and secular spin-spin systems can be considered to be independent, so we can assign a temperature θ_z to this Zeeman Hamiltonian, and θ_d to the secular part of the spin-spin Hamiltonian $\mathcal{H}_d^0$. Immediately before turning on H_1, the spin-spin system is at the lattice temperature θ_l in both the laboratory and the rotating frames, since $\mathcal{H}_d^0$ is the same in the rotating or laboratory frames. On the other hand the Zeeman temperature in the rotating frames is very cold, since we have[5]

$$M_0=CH_0/\theta_l \text{ from the laboratory frame}$$
$$=Ch/\theta_z \text{ from the rotating frame},$$

where C is the Curie constant, $C=N\gamma^2\hbar^2I(I+1)/3k$. Since $H_0\gg h$, $\theta_z\ll\theta_l$. Turning on H_1 couples the dipolar and Zeeman reservoirs together, and they approach the final equilibrium temperature θ. The coupling of H_1 produces transitions which we assume are governed by simple rate equations for the populations of the various states. This assumption is quite common in all cross-relaxation calculations. Provotorov makes it implicitly in his work when he evaluates the relaxation times. As has been shown by Schumacher,[10] when the two systems are characterized by temperatures, the many rate equations for the numerous energy levels reduce to two linear rate equations, one for the time derivative of $1/\theta_z$ and other for that of $1/\theta_d$. But the conservation of energy requires that θ_z and θ_d be related by

$$-Ch^2/\theta_z-CH_L^2/\theta_d=\text{constant}. \tag{13}$$

Equation (13) is thus a first integral, so that one of the resultant time constants is infinite, and a single exponential results. Since $M_z\propto(1/\theta_z)$ this means that M_z relaxes according to a single exponential towards its equilibrium value,

$$M_z-(M_z)_{\text{eq}}=[M_0-(M_z)_{\text{eq}}]e^{-t/\tau}, \tag{14}$$

where we have used the fact that $M_z=M_0$ initially. Taking the derivative of Eq. (14), evaluating it at $t=0$, and comparing this with Eq. (11), which is valid initially where perturbation theory must be correct, we obtain

$$\frac{1}{\tau}=2W(\omega)\frac{M_0}{M_0-(M_z)_{\text{eq}}}. \tag{15}$$

Using Eq. (10) for $(M_z)_{\text{eq}}$, we get

$$\frac{1}{\tau}=2W(\omega)\frac{H_{\text{eff}}^2+H_L^2}{H_1^2+H_L^2(1-h/H_0)}$$
$$=\pi\gamma^2H_1^2f(\omega)\frac{H_{\text{eff}}^2+H_L^2}{H_1^2+H_L^2(1-h/H_0)}. \tag{16}$$

This result is exactly that found by Provotorov,[6] as indeed it must be, since we have made exactly the same approximations. The complete time development of the magnetization is therefore[11]

$$\frac{M_z}{M_0}=\frac{h^2+H_L^2h/H_0}{H_{\text{eff}}^2+H_L^2}+\frac{H_1^2+H_L^2(1-h/H_0)}{H_{\text{eff}}^2+H_L^2}$$
$$\times\exp\left[-\pi\gamma^2H_1^2f(\omega)t\frac{H_{\text{eff}}^2+H_L^2}{H_1^2+H_L^2(1-h/H_0)}\right]. \tag{17}$$

This expression involves the successful integration of the equations of motion well beyond the time $(1/W)$ for which perturbation theory is usually valid. Figure 1

[9] J. Philippot, Phys. Rev. **133**, A371 (1964).

[10] R. T. Schumacher, Phys. Rev. **112**, 837 (1958).

[11] It should be noted that an alternative and equally correct derivation of Eq. (17) can be obtained from the perturbation-theory equation of the power absorption

$$P=\frac{2\pi\omega^2\hbar^3\gamma^2}{k\theta Z}H_{\text{rf}}^2\sum_{a,b}|\langle a|I_x|b\rangle|^2\delta(E_a-E_b-\hbar\omega),$$

where Z is the partition function. If we equate this to the rate of change of energy from the spin-temperature expression,

$$dE/dt=C(H_0^2+H_L^2)/\theta^2,$$

and solve for $\theta(t)$, we find

$$\tau'=\tau\omega^2/\gamma^2(H_0^2+H_L^2).$$

When one deals with a large static field, $H_0\gg H_L$, the discrepancy is negligible. However, when $H_0\approx H_L$, the discrepancy is very large, showing that the perturbation-theory approach to resonance is a high-field theory. We have found in our low-field work that τ' gives a better qualitative description of our data, and have thus used it in calculating our curves.

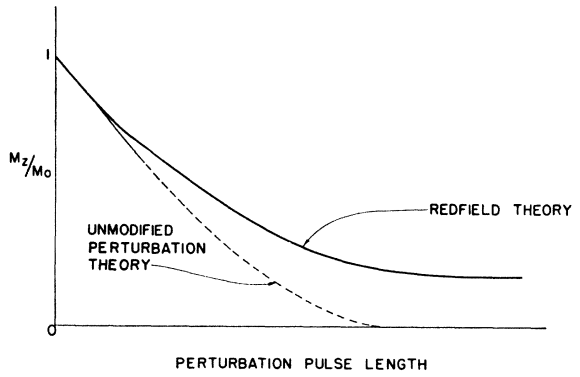

FIG. 1. Time development of the magnetization as a result of saturation for the case of an infinite spin-lattice relaxation time, contrasting the predictions of Redfield with the unmodified perturbation theory of BPP.

contrasts the behavior of the system as a function of time as predicted by Eq. (17) with the simple perturbation-theory prediction of Eq. (7). Goldburg[4] studied the exponential approach to equilibrium for one value of h of a system for which Eq. (17) should be valid and found τ to be in fair agreement with the theoretical value. Walstedt has reported experimental results for one value of t that are in good agreement with his calculations.[7]

As we remarked in the Introduction, our experiments are carried out in the rotating reference frame. The experimental procedure involves bringing M along H_e an adiabatic demagnetization. At exact resonance ($\omega=\gamma H_0$) this puts M along H_1. The alternating field is applied by modulating H_0. We decompose the linearly polarized modulating field into two rotating components of amplitude H_a, and denote the component of H_a perpendicular to $H_{\rm eff}$ as H_{a1}. We neglect the parallel component. We can now transcribe Eq. (17) in the appropriate symbols[11] to find the magnetization M_z, along $H_{\rm eff}$, obtaining

$$M_{z'}=(M_{z'})_{\rm eq}+[M(0)-(M_{z'})_{\rm eq}]\times\exp\left(\frac{-\pi H_{a1}^2\omega_a^2 f'(\omega_a)t}{H_{\rm eff}^2+H_L^2}\frac{1}{1-(M_z')_{\rm eq}/M_0}\right), \quad (18)$$

where

$$(M_{z'})_{\rm eq}=\frac{H_1}{H_{\rm eff}}\frac{h'^2+H_L'^2h'/H_{\rm eff}}{H_{\rm eff}'^2+H_L'^2},$$

and where $M(0)$ is the magnetization along H_1 just after the adiabatic demagnetization. In obtaining Eq. (18), it is useful to envisage a second rotating frame, rotating about $H_{\rm eff}$ at angular frequency ω_a and further defined in Fig. 2. The distance off resonance of the audio field is given by h', and $H_{\rm eff}'$ is the effective static field in the second rotating frame. H_L' is the local field in the second rotating frame. $H_L'=H_L|(3\cos^2\theta-1)/2|$ as explained below. Equation (18) is obtained in a way that is completely analogous to the derivation of Eq. (17).

In order to compare Eq. (18) with experiment, it is necessary to know $f'(\omega_a)$, which describes the transition probability of spins quantized along $H_{\rm eff}$ under the action of the audio field. Fortunately, when $H_{\rm eff}\gg H_L$, $f'(\omega_a)$ is very simply related to $f(\omega)$ which describes the absorption of power from H_1 of spins aligned along H_0. As Goldburg first observed, the breadth of $f'(\omega_a)$ is determined by that part of $\mathcal{H}_d^0$ which commutes with $I_{z'}$, the total component of spin along $H_{\rm eff}$. It is simple to show that this goes as $|(3\cos^2\theta-1)/2|$, where θ is the angle between $H_{\rm eff}$ and H_0. One therefore finds that $f(\omega)$ and $f'(\omega_a)$ have the same shape, but $f'(\omega_a)$ is narrower by the factor $|(3\cos^2\theta-1)/2|$. The problem of finding $f'(\omega_a)$ is thus reduced to a determination of $f(\omega)$. Our experiments were performed using a CaF_2 crystal aligned with the [111] direction parallel to H_0. The results of previous experiments have shown that the line shape is very nearly Gaussian. We can therefore write that

$$f'(\omega)=(2\pi\langle\Delta\omega^2\rangle)^{-1/2}\exp\left(-\frac{(\omega-\omega_0)^2}{2\langle\Delta\omega^2\rangle}\right), \quad (19)$$

where $\omega_0=\gamma H_{\rm eff}$ and $\langle\Delta\omega^2\rangle$ is the second moment in the rotating frame. The second moment can be calculated theoretically by means of Van Vleck's technique.

We note also that by a similar argument H_L' is given by $H_L|(3\cos^2\theta-1)/2|$.

[Lee and Goldburg[12] have recently calculated the first and second moments of the line shape in the rotating frame, including the effects of the $\mathcal{H}_d^0$ which do not commute with I_z. We have also done this calculation[13] using a slightly different approach. One finds two main features, an extreme narrowing of the line at the magic angle, $\cos^2\theta=\frac{1}{3}$, and a shift in the center of gravity of the line as a function of θ. At $\theta=90°$, one finds $\langle\Delta\omega^2\rangle=384\times10^6$ rad^2/sec^2. Our experimental technique, rotary saturation, is not well suited to studying the perturbation region, as we would have to measure very small changes in the magnetization. Lee and Goldburg[12] have checked these predictions using a different method. In their experiments, they measured the free precession of the magnetization about $H_{\rm eff}$, after H_1 is pulsed on. The rate of damping of this precession can be directly related to the second moment of the line shape. The period of the precession can be used to measure the first moment. Their measurement of the second moment was in very good agreement with the calculated value. They found that the line width remaining at the magic angle could be accounted for by considering higher order terms. They did not, however, find the frequency shift predicted by the first-moment calculation, possibly because of insufficient experimental sensitivity.]

[12] M. Lee and W. I. Goldburg, Phys. Rev. **140**, A1261 (1965); M. Leek, thesis, University of Pittsburgh (unpublished).

[13] J. R. Franz, thesis, University of Illinois (unpublished).

A. Low-Field Case

We now discuss the case in which the effective static field in the first rotating frame is of the order of or smaller than the local field. In the previous section, we pointed out that in this case Redfield theory should fail, since the transformed Hamiltonian is actually more time-dependent than the original one. The only simple assumption one can then make is that a spin temperature θ will be established in the first rotating frame, and that the system will absorb energy from the audio field, causing the magnetization and $(1/\theta)$ to go exponentially to zero.[8]

Since, as we have mentioned, we start our experiments with the system in the first rotating frame, we also use the Hamiltonian in the first rotating frame to calculate our results. Then considering the case of $\theta=90°$, (H_{eff} exactly at resonance) we have

$$\mathcal{H}=\sum_{k>j}A_{jk}[\mathbf{I}_j\cdot\mathbf{I}_k-3I_{jz}I_{kz}]-\gamma\hbar H_1\sum_j I_{jx}-\gamma\hbar 2H_a\sum_j I_{jz}\cos\omega_a t. \quad (20)$$

This is an unusual Hamiltonian. The dominant term is now the spin-spin interaction term while added to this are two perturbation terms, one static, one time-dependent. The time-dependent term is the term capable of causing transitions. However, it commutes with the spin-spin term and therefore would have no effect on the system if a small rf field were not present to mix the levels. Thus we expect the rate of transitions to be proportional to both H_1^2 and H_a^2. For this reason, the situation we are describing differs markedly from that of nonresonant spin absorption.[8]

To calculate directly the effect of the audio field on the system described by the above Hamiltonian is very difficult. The first step would be to calculate the amount of mixing caused by the rf field, but since the unperturbed eigenfunctions and eigenvalues of the system are those of the spin-spin Hamiltonian and, therefore, unknown, this cannot be done. Instead we transform the Hamiltonian in such a way that the new time-dependent term can cause transitions between the unperturbed states. We define a new wave function ψ' where $\psi=R\psi'$ and

$$R=\exp\left[i\gamma 2H_a I_z\int_0^t\cos\omega_a t'dt'\right]. \quad (21)$$

Substituting in Eq. (20), we find a new Schrödinger equation with a new Hamiltonian $\mathcal{H}'$

$$\mathcal{H}'=\sum_{k>j}A_{jk}[\mathbf{I}_j\cdot\mathbf{I}_k-3I_{jz}I_{kz}]-\gamma\hbar H_1\sum_i\left\{I_{jx}\cos\left(\frac{2\gamma H_a}{\omega_a}\sin\omega_a t\right)-I_{jy}\sin\left(\frac{2\gamma H_a}{\omega_a}\sin\omega_a t\right)\right\}. \quad (22)$$

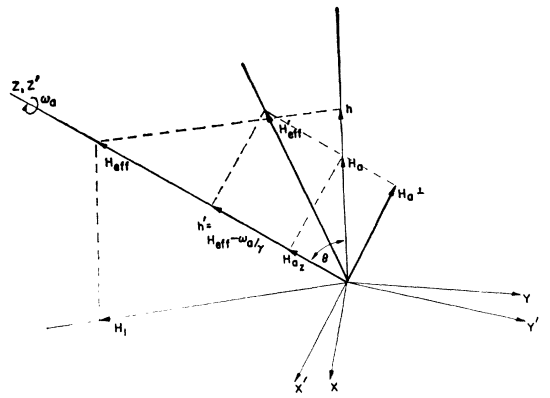

FIG. 2. The second rotating frame. (Symbols defined in the text.)

For $\gamma H_a\ll\omega_a$, we can expand the expression in the brackets and keep only the lowest order terms. This is not a severe restriction experimentally, since it is easy to work with weak audio fields. Then we find

$$\mathcal{H}'=\sum_{k>j}A_{jk}[\mathbf{I}_j\cdot\mathbf{I}_k-3I_{jz}I_{kz}]-\gamma\hbar H_1\sum_j I_{jx}+\frac{2\gamma^2\hbar H_1H_a}{\omega_a}\sin\omega_a t\sum_j I_{jy}. \quad (23)$$

The time-dependent term is now proportional to both H_1 and H_a. Since it no longer commutes with the spin-spin term, it can cause direct transitions between the unperturbed levels of the spin-spin system. This is equivalent to applying a perturbing field of amplitude $2\gamma H_1H_a/\omega_a$ in the y direction, so we can use perturbation theory to calculate the rate at which the system is heated by the audio field. Then we have

$$W(\omega)=(\pi\gamma^4H_1^2H_a^2/2\omega_a^2)f(\omega_a), \quad (24)$$

where $f(\omega_a)$ is the normalized shape function describing the absorption of audio energy. Using Eq. (24), we get

$$M_z=M_0e^{-2W(\omega)t}=M_0\exp[-(\pi\gamma^4H_1^2H_a^2/\omega_a^2)f(\omega_a)t] \quad (25)$$

for $\gamma H_a\ll\omega$.

III. EXPERIMENTAL PROCEDURE AND APPARATUS

A. Procedure

The technique of rotary saturation was developed by Redfield.[3] To perform a rotary-saturation experiment, it is necessary to add an audio-frequency channel to a standard nuclear-resonance apparatus. The audio channel is used to probe spin systems in the rotating frame where the spins are quantized along an effective static field $H_{\text{eff}}=[H_1^2+(H_0-\omega/\gamma)^2]^{1/2}$. Since the audio field H_a is created in the laboratory frame but viewed in the rotating frame, it is convenient to align H_a with the one axis shared by these two frames, the axis of the laboratory static field H_0.

Redfield performed his original experiments using a

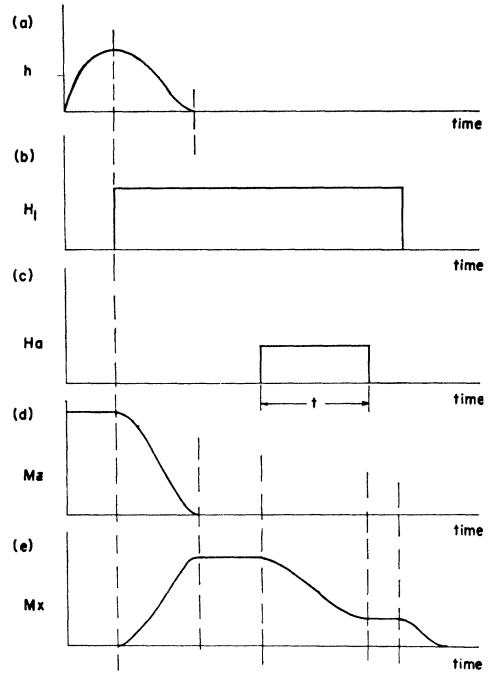

FIG. 3. Time dependence of magnetic fields (h, H_1, and H_a) and the resulting magnetization components M_z and M_x.

steady-state apparatus. He used field modulation with lock-in amplification and detection to enhance his signal-to-noise ratio. Our experiments have utilized pulse methods and a boxcar integrator, the pulse analog of lock-in detection. One advantage of pulse equipment is that we can study nonequilibrium phenomena in a straightforward manner. We simply use a short pulse and make measurements immediately after the pulse is turned off. However, for spin systems that are only weakly coupled to the lattice, i.e., long T_1, pulse techniques become inefficient since one must wait times of the order of T_1 between measurements.

The pulse sequence used in our experiments is shown in Fig. 3. The spin system, consisting of the fluorine nuclei in CaF_2, is allowed to come to equilibrium in the laboratory frame in the presence of H_0, so that a large magnetization develops. The static field is then pulsed away from the resonant value an amount $h \approx 15$ G and the rf field H_1 is pulsed on. When h is adiabatically decreased to zero, the magnetization remains aligned along the effective static field in the rotating frame as it approaches H_1. At the end of this process the magnetization is aligned along H_1 in the rotating frame. If we wish to perform experiments at some value of the angle $\theta = \tan^{-1} H_1/h$ other than $\theta = 90°$, we accomplish this by ending the adiabatic change in h before h becomes zero. After the Zeeman and spin-spin systems have had time to re-equilibrate in the rotating frame, the audio field H_a is pulsed on, allowed to remain on for a variable time t and then pulsed off. The magnetization precesses about H_{eff}, and after the component transverse to H_{eff} has had time to dephase, H_1 is pulsed off. The remaining magnetization precesses about H_0 and is detected before it decays appreciably. The pulse sequence is repeated every 10 sec. A curve is traced out by varying ω_a through the resonant value $\omega_a = \gamma H_{\text{eff}}$. Measurements can be made to study the effect of varying H_1, H_a, t, and the angle θ. All experiments were performed at room temperature.

B. Apparatus

The crossed-coil pulsed-NMR apparatus we used was essentially the same as that described by Ailion.[14] A block diagram of the apparatus is shown in Fig. 4. A continuous wave (cw), 7.5-Mc/sec signal, produced by a crystal oscillator, is fed into a gated amplifier. The pulsed output is then amplified by a three-stage, class C, power amplifier, and passes through a coupling network to the transmitter coils. The signal produced by the precessing nuclei is picked up by the receiver coil, and passes through a low-noise preamplifier and high-gain rf amplifier to the detector. Since the alignment of the crossed coils is not perfect, there is pickup from the transmitter coils, and the amplifier is blocked for the duration of the rf pulses. The recovery time of our amplifier is about 15 μsec. A coherent detection scheme is used, so that the output of the detector is the envelope of the magnetization decay pattern. This is viewed directly with an oscilloscope and is also fed into a two-channel boxcar integrator.[14] The boxcar compares the signal at the beginning of the decay to the base line, eliminating base-line drift problems, and allows us to average over many pulses. The output of the boxcar goes directly to a recorder, so that a permanent record of the signal height is automatically produced.

The audio channel consists of an oscillator and a push-pull audio amplifier of variable output impedance. Audio pulses are produced by modulating the screens of the last stage of the amplifier. The audio coils are wrapped on the outside of the rf probe. Fields up to a few gauss can be produced without distortion.

The timing of the various pulses is controlled by a network of Tektronix pulse and waveform generators. The controlling pulses are viewed on a dual-trace oscilloscope and can be continuously monitored.

The nuclei studied were the F nuclei in a single crystal of CaF_2. CaF_2 is a face-centered cubic crystal with the basis having a calcium atom at 000 and the fluorine atoms at $\frac{111}{444}$ and $\frac{333}{444}$. CaF_2 was chosen as the sample because many previous experiments had shown that all of the high-field line-shape theoretical predictions were well satisfied. Only one magnetic species must be considered since the calcium nuclei have spin 0. Moreover, since the fluorine nuclei have spin $\frac{1}{2}$, quadrupole effects are absent. The spin-lattice relaxation time of our sample of CaF_2 was about 12 sec. The CaF_2 crystal was

[14] D. C. Ailion, thesis, University of Illinois (unpublished).

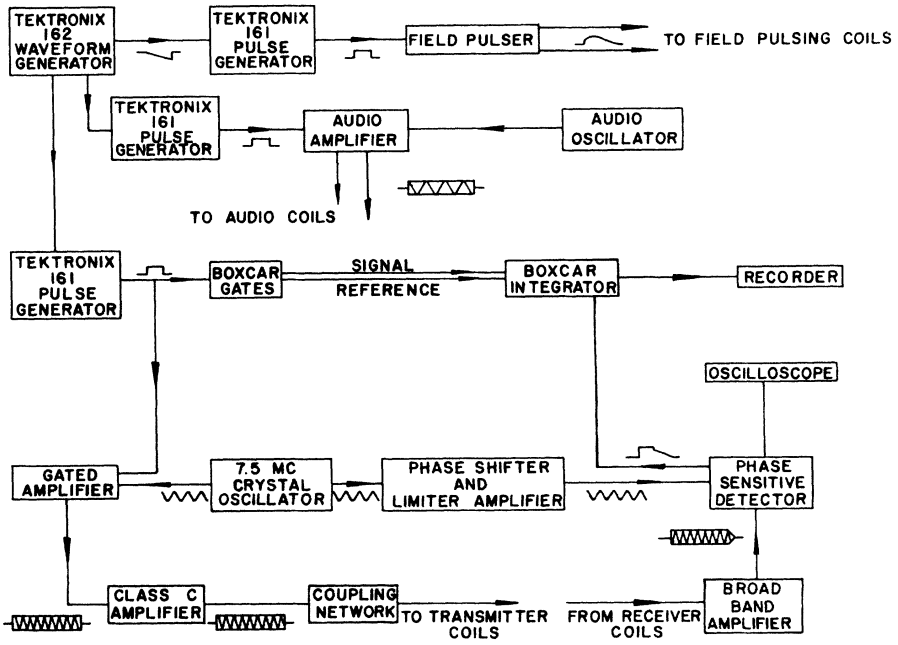

FIG. 4. Block diagram of the apparatus.

aligned such that the [111] direction was approximately parallel to the magnetic field H_0. After the crystal was aligned, we measured H_L, the local field in the first rotating frame, and found it to be 0.90 ± 0.01 G, in agreement with the calculated value.

The rf fields used during the experiments reported in this paper ranged from 0.1 to 6 G. A small fraction of the voltage across the transmitter coils was viewed on an oscilloscope, allowing a relative determination of H_1. The amplitude of H_1 in gauss was obtained using a glycerin sample by measuring the length of 180°, 360°, 540°, etc., pulses and using the equation $\gamma H_1 t = n\pi$. Unfortunately, the glycerin sample had a slightly different geometry from the CaF_2 sample, so the calibration has an uncertainty of about 5%.

The audio-field amplitude was calibrated in a completely analogous way using glycerin, the main difference being that the pulses were now applied in the *second* rotating frame. The oscillation of the signal height as a function of the length of the audio pulse provided the most direct verification of the quantization of the spins in the second rotating frame. The frequency of the audio-field pulses was calibrated using a Hewlett-Packard cycle counter.

The inhomogeneity in H_0 was checked by measuring the time constant of the free induction decay following the turn-off of H_1, using a liquid sample. The time constant measured was 2 msec. From this, we can calculate the frequency spread, $\langle\Delta\omega^2\rangle^{1/2}$, of the line, caused by H_0 inhomogeneity, to be about 250 cycles/sec for protons or about 1/20 of a gauss.

The H_1 inhomogeneity was determined by measuring the duration of the free precession signal about H_1. (If H_1 is pulsed on suddenly, the magnetization precesses about H_1 in the rotating frame. For a liquid sample, the magnetization dephases in a time that is determined by the H_1 inhomogentity.) In this way, we were able to estimate that the inhomogeneity was about 4%.

As we will mention later, we found that our experimental rotary-saturation line shapes were asymmetric, having a longer tail on the low-field side. We wished to check to see if the asymmetry could be caused by the H_1 inhomogeneity. To do this, we searched for that higher order term in the magnetic potential that satisfied Laplace's equation and gave the lowest order field spread. Using the geometry of our sample we calculated a distribution curve showing the number of spins which experienced various values of H_1. We found that the distribution had a long tail on the low-field side, which was caused by the sample being long compared to the cross-sectional dimensions. We therefore attributed the asymmetry of our experimental curves to the distribution of the H_1 inhomogeneity. After the experiments reported in this paper were completed, we replaced the sample with one only half as long and remeasured the line shape finding, as expected, that most of the asymmetry had disappeared.

IV. EXPERIMENTAL RESULTS

A. High-H_1 Case

When $H_1 \gg H_L'$, we are dealing with the high-field case and the results are given by Eq. (18). There are three particular points we wish to verify experimentally. The first is that the equilibrium magnetization produced by a long audio pulse is given correctly by the Redfield theory applied in the second rotating frame. The second is that the variation in effective local field with θ, the

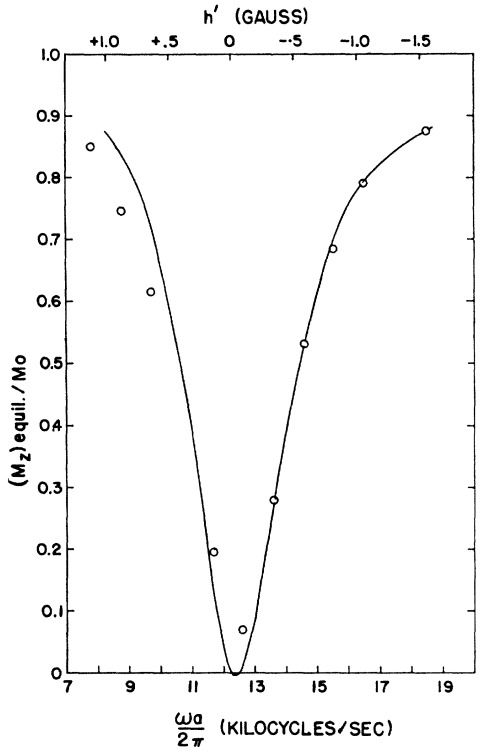

FIG. 5. The fraction of magnetization remaining after an audio pulse of frequency $\omega_a/2\pi$ that is long enough to allow the system to reach an equilibrium in the second rotating frame. The experimental points were taken with $\theta=90°$, $H_1=3.05\pm0.10$ G, and $H_a=0.08\pm0.005$ G. The solid line is a plot of the theoretical Eq. (18) with no adjustable parameters.

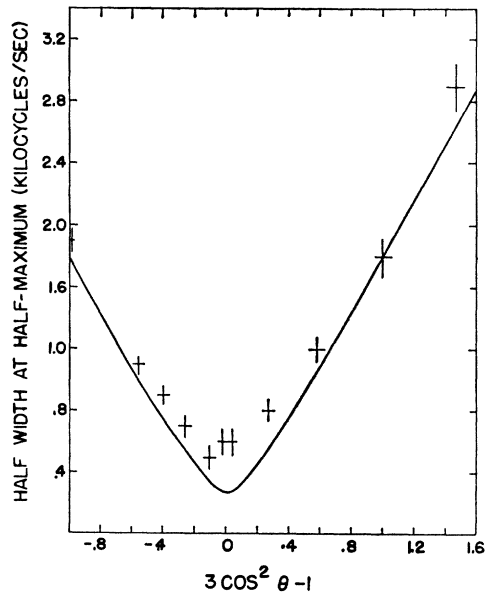

FIG. 6. The half-width at half-maximum of the rotary-saturation curves as a function of $3\cos^2\theta-1$. The experimental points were taken with $H_1=3.1\pm0.1$ G and $H_a=0.08$ G. The solid line shows the theoretical prediction with no adjustable parameters. The predicted width at $3\cos^2\theta=1$ is caused entirely by the presence of the audio-frequency field.

angle between H_{eff} and H_0, is correctly given by the formula $H_L'=H_L|(3\cos^2\theta'-\frac{1}{2}|$ and thus vanishes at the magic angle for which $\cos^2\theta=\frac{1}{3}$. The third is that the time evolution of the system towards the equilibrium is correctly described by a Provotorov theory.

We turn first to a discussion of the equilibrium. After the audio pulse has remained on long enough for the system to reach an equilibrium in the second rotating frame, the magnetization should be given by the first term in Eq. (18). Thus the magnetization is expected to go to zero when ω_a is right at resonance since there $h'=0$. If a curve is traced out by varying ω_a, the curve will be asymmetric since the term linear in h' will change sign as ω_a passes through the resonance condition. Figure 5 shows a set of experimental points taken for $(M_z)_{\text{eq}}/M(0)$ as a function of $\omega_a/2\pi$ plus a plot of the first term in Eq. (18) in which there are no adjustable parameters. The experimental points agree fairly well with the theoretical prediction; however, at low frequencies the points fall somewhat below the theoretical curve. As we discussed in the experimental section, this discrepancy is caused by an asymmetric inhomogeneity of the rf field. It can be shown that this inhomogeneity will also prevent complete destruction of the magnetization at $\omega_a=\gamma H_{\text{eff}}$.

To check the second point (the θ dependence of H_L') we ran similar curves at other values of the angle θ

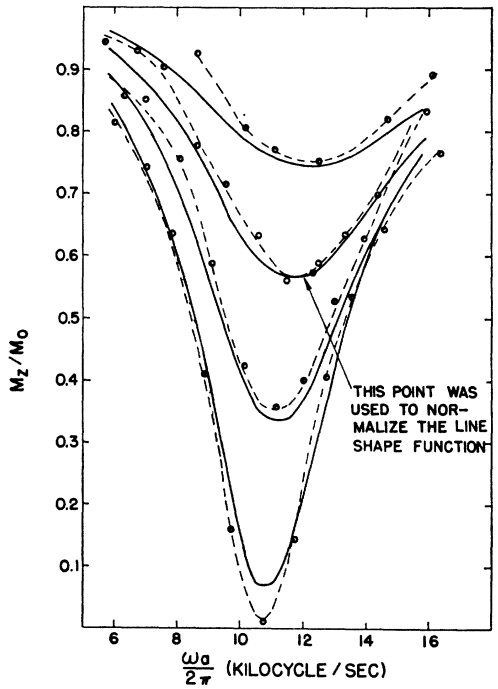

FIG. 7. The fraction of magnetization remaining after audio pulses of frequency $\omega_a/2\pi$, for four different pulse lengths $t=1$, 2, 4, and 10 msec. The dashed lines connect the experimental points. The solid lines are plots of the theoretical Eq. (18) with one adjustable parameter. Experimental conditions were $\theta=90°$, $H_1=2.6\pm0.1$ G, $H_a=0.11\pm0.005$ G.

between the effective field and H_0 to determine how the widths of the curves varied. From Eq. (18) one finds that the half-width at half-maximum should be approximately $\gamma(H_L'^2+H_{a1}^2)^{1/2}$, where $H_L'=H_L'(90°)|3\cos^2\theta-1|$. Figure 6 shows the expected width as a function of $|3\cos^2-1|$, together with our experimental results. Because of the large effect of H_1 inhomogeneity on the low-frequency side of the curves, we have used the high-frequency side to obtain the points shown. The agreement is excellent except at $H_L'=0$, where we expect from the work of Lee and Goldburg[12] that higher order contributions to H_L' from the nonsecular terms in the Hamiltonian dominate.

The third point we wish to check is that the time evolution of the magnetization follows the Provotorov equation. In principle we have no adjustable parameters in the time constant, but since errors in line breadth or the calibration of H_a would systematically displace the curves, we chose rather to fit the data by normalizing at one point. The normalization point is indicated on Fig. 7 which shows M_z/M_0 as a function of $\omega_a/2\pi$ for four durations of the audio pulse.

One interesting feature which shows up is that the frequency of maximum destruction is displaced downwards for the longer duration pulses. going from 12.1 kc/sec for the shortest duration to 10.7 kc/sec for the longest. This shift can be explained as follows.[11] (In so doing we are invoking corrections of order H_L^2/H_1 and have no assurance that there are no other terms than those we include, also of this order. However, our computation shows that some such explanation should be successful.) For short pulses the greatest destruction of magnetization occurs where $\omega^2 f(\omega)$ is a maximum. Using a Gaussian distribution, one finds the maximum at $\omega_a^2=\omega_1^2+8\langle\Delta\omega^2\rangle/2$ where $\omega_1=\gamma H_1$, giving $\omega_a/2\pi=12.1$ kc/sec .For long pulses, the destruction is greatest when $(M_z)_{eq}$ is a minimum, that is,

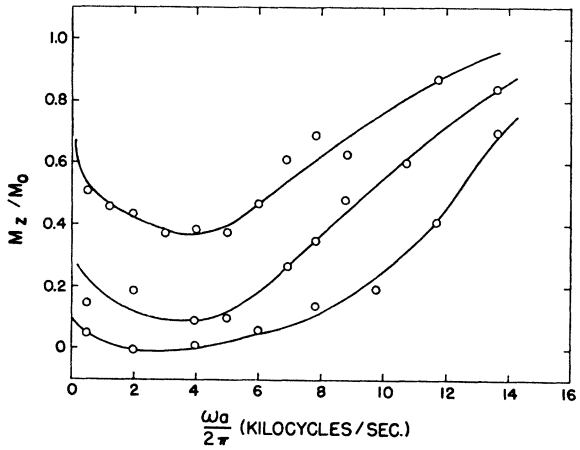

FIG. 8. The low-H_1 case: The fraction of magnetization remaining after an audio pulse of frequency $\omega_a/2\pi$ for pulse lengths of 20, 40, and 80 msec. The lines were drawn to connect the experimental points, $\theta=90°$, $H_1=0.37$ G, $H_a=0.10$ G.

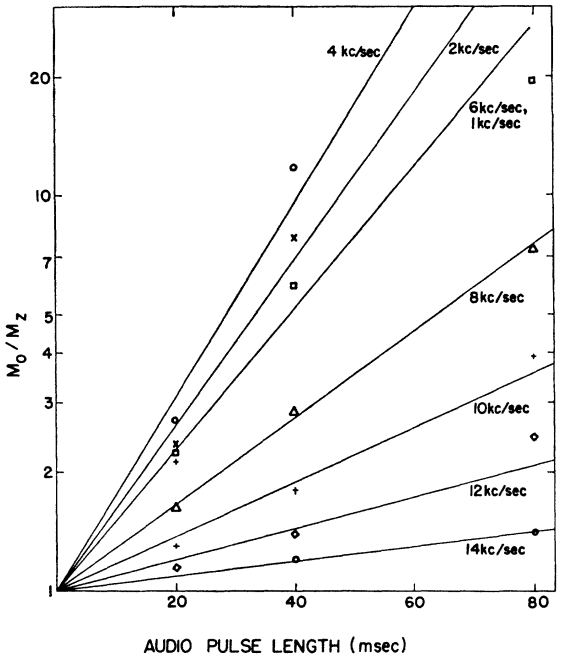

FIG. 9. Low-H_1 case: The fraction of magnetization remaining after an audio-frequency pulse as a function of audio pulse length for various values of ω_a. The points are taken from Fig. 8.

when $h'=-H_L'^2/H_1$ or when $\omega_a=\omega_1+(\gamma H_L'^2/H_1)=10.7$ kc/sec.

The general features of the experimental curves, including the dramatic change of shape as well as the relative time dependence are clearly well described by Eq. (18). If one has a calibration of H_a, one can also predict the actual slopes (not just relative slopes). E. A. S. Lewis of our laboratory has made a careful study of the slopes for the various H_1's. H_a was calibrated using a liquid sample, by applying H_a for pulses of variable duration so as to generate π, 2π, etc., pulses. In this manner, at an H_1 of 3.05 G, he verified the absolute magnitude of the slope within experimental error ($\pm 15\%$).

It is important to recognize that a measurement of the slope dM_z/dt for short times does not give one any information on whether or not spin temperature concepts in the rotating frame are valid since, as we have seen, the region of small destruction can be analyzed solely using perturbation theory. The fact that a single exponential describes the approach to equilibrium is a test of (a) the concept of linear rate equations and (b) that two spin temperatures (θ_z and θ_d) describe the spin system. The fact that the correct equilibrium curve is predicted is a test of the applicability of Redfield theory.

B. Low-H_1 Case

As we have remarked, when $H_1<H_L'$, the Redfield transformation to a second rotating frame no longer

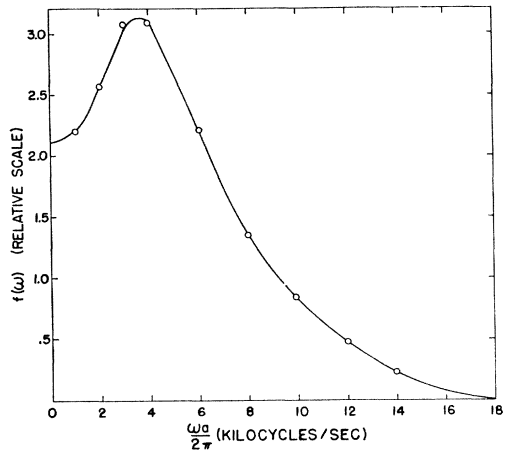

FIG. 10. Low-H_1 case: The line-shape function $f(\omega_a)$ deduced from the slopes of the lines of Fig. 9.

gives a time-independent Hamiltonian. One would most naturally view the problem in the first rotating frame, keeping $\mathcal{H}_d^0$ time-independent. For times longer than $1/W(\omega_a)$, where $W(\omega_a)$ is the transition probability of a spin under the action of the audio field H_a, we cannot be sure whether or not perturbation theory is correct. What we find is shown in Fig. 8, which shows experimental curves for M_z/M_0 as a function of $\omega_a/2\pi$ for three different durations of the audio pulse. The experimental data were taken with $H_1=0.37\pm0.01$ G and $H_a=0.10\pm0.005$ G. These curves show clearly that for any frequency ω_a, the equilibrium corresponds to complete destruction of the signal as in a BPP theory in sharp contrast to what is found in Fig. 7 where the equilibrium is given by a Redfield theory.

In order to demonstrate that in the low-field case the equation of motion is really a simple exponential, we show the same data in Fig. 9 where we have plotted $\ln(M_0/M_z)$ as a function of time. It can be seen that the points taken for a given frequency fall on a straight line within the experimental scatter. The slopes of these lines are proportional to $f(\omega)$, so it is easy to find the line shape from this data. This is shown in Fig. 10.

Of course, this line shape is not the same as that in high H_1. We do not, in fact, know it. However we can compute its moments. In order to compare this line shape with theoretical predictions, we made a numerical calculation of the second moment about zero frequency, $\langle\omega^2\rangle$, from the curve in Fig. 10 and found

$$\langle\omega^2\rangle/4\pi^2=37.7\pm3.0\ \text{kc}^2/\text{sec}^2.$$

Calculating $\langle\omega^2\rangle$ in the standard way,[15] we find

$$\langle\omega^2\rangle=-\frac{1}{\hbar^2}\frac{\text{Tr}[\mathcal{H},I_y]^2}{\text{Tr}I_y^2}$$
$$=3\gamma^2H_L^2+\gamma^2H_1^2$$
$$=40.8\pm0.8\ \text{kc}^2/\text{sec}^2,$$

where the uncertainty arises from the experimental precision in calibrating H_1. We feel that the agreement confirms our analysis that the nuclear resonance at very low static fields is given correctly by a BPP theory.

C. Miscellaneous Other Effects of Practical Significance

In the previous two sections we have compared theory and experiment for both high and low H_1, but for low audio fields H_a. We now turn to two other effects of practical significance to people observing rotary-saturation experiments. The first has to do with the practical question of using rotary saturation to calibrate the strength of H_1, when H_1 is not very much bigger than H_L. The second has to do with extra features observed in the rotary-saturation spectrum when H_a becomes comparable to H_L.

1. Location of Maximum Destruction

In a rotary-saturation experiment, the line width of the saturation is often comparable to the central frequency ($H_1\approx H_L$). The accuracy of the basic resonance equation $\omega_a=\gamma H_1$ is therefore brought into question. Since many people are currently using rotary saturation to calibrate rf fields, we thought it would be useful to check the accuracy of such a calibration. Figure 11 shows the results of our study, carried out at resonance ($\theta=90°$). The points would fall on the straight line $\omega_a=\gamma H_1$ if there were no correction arising from the line breadth. One can see that the simple equation

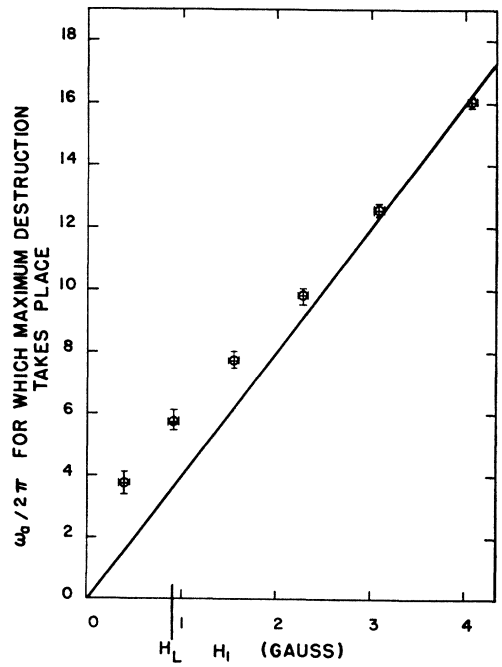

FIG. 11. Audio frequency $\omega_a/2\pi$ of maximum destruction versus H_1. The solid curve is a plot of the equation $\omega_a=\gamma H_1$.

[15] A. Abragam, *The Principles of Nuclear Magnetism* (Oxford University Press, London, 1961), Chap. IV.

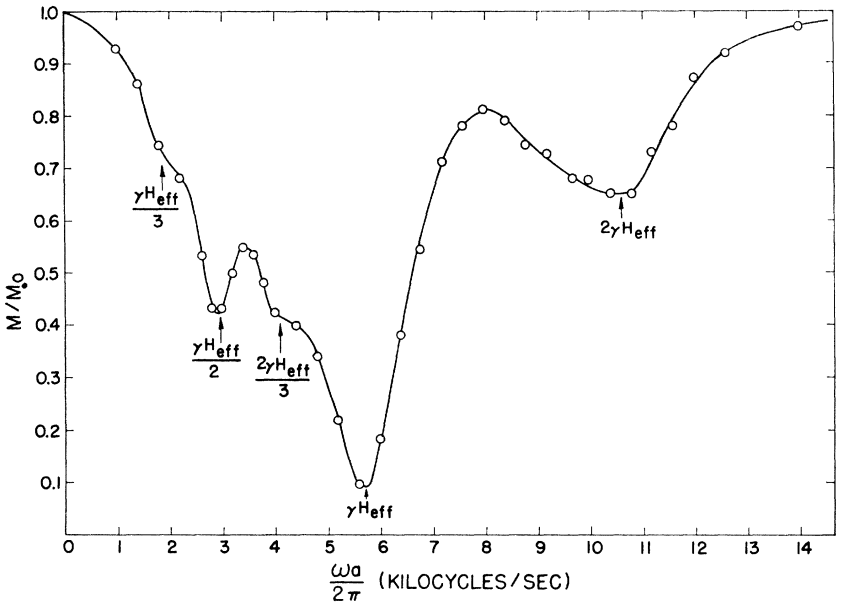

FIG. 12. The rotary-saturation experiment showing one-, two-, and three-quanta transitions $\theta=65°$, $H_{\text{eff}}=3.4\pm0.1$ G, $H_a=0.80\pm0.05$ G.

is accurate to better than 10% if $H_1>2H_L$, where H_L is the local field calculated from the full rotating frame spin-spin Hamiltonian. The points on the graph were taken from rotary-saturation curves where essentially complete destruction occurred for the frequencies shown, i.e., for equilibrium. We have already pointed out that there is a decided frequency shift between the maximum destruction of curves taken in the perturbation-theory region and those taken in the Redfield equilibrium region (see Fig. 7).

There are many reasons why rotary saturation is not an accurate calibration technique when $H_1\approx H_L$. The most important is that as H_1 approaches H_L, the field experienced by a nucleus, $(H_1^2+H_L^2)^{1/2}$, is strongly dependent on H_L, shifting the dip in the curves to higher frequencies. It is possible to correct for such a shift, but for $H_1\approx H_L$, it is unclear just what one should include in the local field value. For $H_1\gg H_L$, it is clear that only the secular part of the rotating frame spin-spin Hamiltonian should be included, since the nonsecular terms oscillate at a frequency far off resonance in the second rotating frame. It is also clear that for $H_1<H_L$, the full spin-spin Hamiltonian will contribute to the local field, for in this case the spin-spin interaction is actually the dominant term in the Hamiltonian. But for $H_1\approx H_L$, the local field is not a well defined quantity. One also finds that as H_1 approaches H_L, the rotary-saturation lines become very broad and asymmetric (see Fig. 8), so that there is a large uncertainty in choosing the point of maximum destruction. Even if $H_1>H_L$, one expects a small shift to higher frequencies, as is evident in Eq. (18), which is caused by the redistribution of the energy originally stored in the spin-spin interaction. If $H_1\approx H_a$, one must correct for the Block-Siegert shift.

2. *Many-Quanta Transitions*

During the course of the rotary-saturation experiments discussed in the previous sections, we noticed that for audio-frequency fields of about 0.2 G, a considerable amount of magnetization was destroyed when audio frequency was equal to $(\frac{1}{2})\gamma H_{\text{eff}}$. After measuring the harmonic content of the field created in our audio-frequency coils and finding it negligible, we decided that we were seeing two-quanta transitions, that is, transitions in which two quanta, each of energy $(\frac{1}{2})\hbar\gamma H_{\text{eff}}$, were involved in causing a nucleus to jump to an energy level separated by $\hbar\gamma H_{\text{eff}}$ from its original level. When we increased the strength of the audio-frequency field, we could see resonance lines at $(\frac{1}{3})\gamma H_{\text{eff}}$ and $(\frac{2}{3})\gamma H_{\text{eff}}$, implying the occurrence of three-quanta transitions. The complete rotary-saturation spectrum, obtained with a sample of powdered lithium metal, is shown in Fig. 12. The data were taken with $H_{\text{eff}}=3.4\pm0.1$ G, $H_a=0.80\pm0.05$ G, and $\theta=65°$.

The first two-quanta transition were seen by Hughes and Grabner[16] in 1950, in a molecular beam resonance experiment performed to study the quadrupole hyperfine spectrum of RbF. Bloembergen and Sorokin have analyzed double quantum transitions in nuclear double resonance.[17] More recently Wilking[18] reported the observation of n-quanta transitions between the nuclear Zeeman levels of protons in water, where n was as high as 180. Many-quanta transitions in solids differ from those in liquids and gases in that in solids these transitions can have a high probability of involving at least

[16] V. Hughes and L. Grabner, Phys. Rev. **79**, 314 (1950); **79**, 829 (1950).
[17] N. Bloembergen and P. D. Sorokin, Phys. Rev. **110**, 865 (1958).
[18] S. Wilking, Z. Physik **173**, 490 (1963).

two spins. This is the case when the static magnetic field used in performing the resonance experiments is of the order of or slightly larger than the local field, so that the spins couple as strongly to each other as to the static field. The existence of 2-spin, 3-quanta transitions is proved by the line we see at $\frac{2}{3}H_{\text{eff}}$, which could not occur if only one spin were involved.

One finds that 2-quanta transitions will contribute to resonance lines at $\omega=0$, $\frac{1}{2}\gamma H_{\text{eff}}$, γH_{eff}, and $\frac{3}{2}\gamma H_{\text{eff}}$. We have calculated[13] the transition probability for the line at $\frac{1}{2}\gamma H_{\text{eff}}$ by means of second-order time-dependent perturbation theory. We have included transitions in which two spins take part, by calculating the mixing of the energy levels caused by a first-order spin-spin interaction. There are over 200 different matrix elements that contribute to this transition probability. Combining these matrix elements, one finds

$$W=\frac{\pi}{2}\frac{^2\gamma^2H_a^4}{H_{\text{eff}}^2}\left(\tfrac{2}{3}\sin^2\theta\cos^2\theta+\frac{H_L^2}{H_{\text{eff}}^2}\right.$$
$$\left.\times[20\sin^6\theta\cos^2\theta-24\sin^4\theta\cos^4\theta]\right)(\Delta E-2\hbar\omega). \quad (26)$$

We see that the transition probability is zero when H_1 is exactly at resonance ($\theta=90°$). A simple test of our 2-quanta calculation is to compare the strength of the transition at $\frac{1}{2}\gamma H_{\text{eff}}$ to that of the single-quantum line at $2\gamma H_{\text{eff}}$. This line has been investigated previously by Anderson.[8] Theoretical calculations involving the strength of this line were done by Broer[19] and Wright.[20] For the data in Fig. 12, our calculation predicts that the strength of the $\frac{1}{2}\gamma H_{\text{eff}}$ line will be approximately twice that at $2\gamma H_{\text{eff}}$. From the figure, one finds that the line at $\frac{1}{2}\gamma H_{\text{eff}}$ is about one and one-half times as strong as that at $2\gamma H_{\text{eff}}$. This is good agreement, since the calculation is only approximate.

Calculations for the 3-quanta transition probability were not carried out. However, it is possible to draw qualitative conclusions from examining the types of terms involved. In this way one can predict that the line at $\frac{2}{3}\gamma H_{\text{eff}}$ should not be seen exactly at resonance,

[19] L. J. F. Broer, Physica **10**, 801 (1943).
[20] Arianni Wright, Phys. Rev. **76**, 1826 (1949).

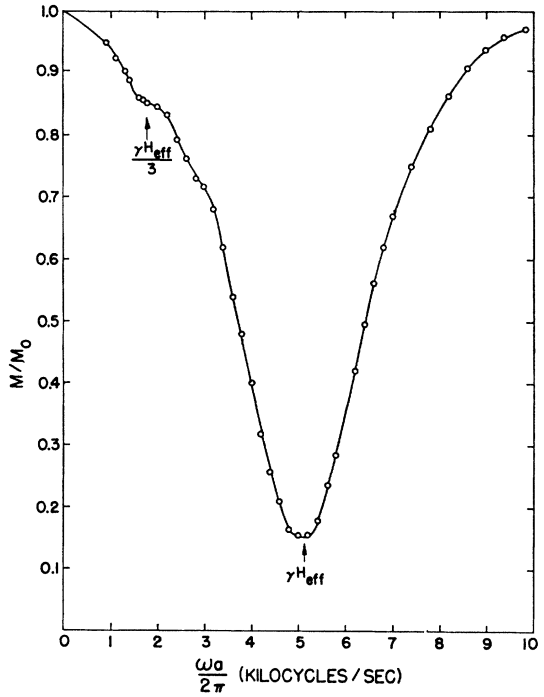

FIG. 13. The rotary saturation spectrum at $\theta=90°$, showing desctuction of magnetization at $H_{\text{eff}}/3$ but none at $2H_{\text{eff}}/3$. Experimental parameters: $H_1=3.1\pm0.1$ G, $H_a=0.85\pm0.05$ G.

but that the line at $\frac{1}{3}\gamma H_{\text{eff}}$ should appear to some extent at all angles provided a large enough audio-frequency field is used. These features were confirmed in our experiments. Figure 13 shows a curve taken for the lithium sample at resonance with $H_{\text{eff}}=3.1\pm0.1$ G and $H_a=0.85\pm0.05$ G, in which only the $\frac{1}{3}\gamma H_{\text{eff}}$ line appears. On the other hand, Fig. 12, taken at $\theta=65°$, shows the presence of all the lines.

ACKNOWLEDGMENTS

It is a pleasure to acknowledge numerous helpful discussions with Dr. P. R. Moran and J. H. Pifer. We are especially indebted to E. A. S. Lewis for his studies which verified the absolute magnitude of the initial slopes associated with Fig. 7.